Towards the Optimal Control of an Active Mechanical Motion Rectifier Power Take-off using Dynamic Programming

Lisheng Yang, Xiaofan Li, and Lei Zuo

Abstract— This paper presents a numerical method to approximately solve a challenging optimal control problem arising from a new mechanical power take-off design. The active mechanical motion rectifier design, while possessing great potential for converting energy from an oscillating mechanical structure, poses a complex control problem where the switching times and control variables need to be optimized simultaneously subject to implicit constraints from rectification requirements. A novel method is proposed to approximate the optimal solution based on dynamic programming (DP) techniques. By discretizing the state space and the control horizon, a new multistep forward dynamic programming scheme is proposed to efficiently incorporate the switching time decisions into the conventional optimization of control variables. The proposed method is flexible enough to accommodate nonlinear dynamics and complex dynamic constraints. A numerical example demonstrated the effectiveness of the proposed method by controlling the active mechanical motion rectifier power take-off for an ocean wave energy converter.

I. INTRODUCTION

Harvesting energy from vibrational mechanical structures is a prospering research area with applications to different fields. Power take-off (PTO) is a critical component for vibration energy harvesters which refers to the mechanical mechanism and transducers that convert the source vibration energy to electricity. For large scale energy harvesters, PTO generally is comprised of a transmission system and an electric generator. For example, wave energy converters (WEC) have used both hydraulic and mechanical transmissions to drive generators from the oscillatory motion of a wave capture structure [1,2]. For large generators, experiments show their efficiency rapidly decreases when their speeds drop below certain ranges [3]. Since vibrational energy sources such as ocean waves always induce oscillatory motions of the harvester structure, generators directly connected to such structures have to frequently reverse rotational directions and cross into the low-speed low-efficiency zones. To increase the generator's efficiency, motion rectification mechanisms are designed to keep the generator's rotation unidirectional above thresholds. The most common rectification mechanisms are hydraulic rectification circuits, which are especially suitable for large scale harvesters due to their high power density [4]. However, employing complex hydraulic circuits introduces additional losses in the transmission and the gain on the generator efficiency may be offset. Compared with hydraulic transmissions, mechanical transmissions involving only rigid body drivetrains are more efficient.

Therefore, mechanical motion rectifiers (MMR) are designed to further increase the PTO's efficiency. Since the first prototype of MMR was designed and tested [5], it has been used in various energy harvesters including regenerative shock absorbers, backpacks, road pavements, and wave energy Although successfully increasing PTO's converters. MMRs have the drawback of limited efficiency, controllability, which hinders their potential for large scale renewable energy applications where control is often needed to achieve economic feasibility [6]. Recently, a new generation of MMR was proposed and designed to enhance the controllability of the PTO [7]. This active mechanical motion rectifier (AMMR) design allows bidirectional force transmission and active rectification switching, eliminating some constraints posed by previous passive MMR designs. Still, designing an optimal controller for the AMMR remains challenging, mainly due to system switching and the inevitable loss of controllability when the generator is disconnected from the oscillating structure.

While there have been some works trying to solve optimal control problems for switching systems [8-11], they assume the system can be controlled for each switched subsystem. For systems using the AMMR PTO, control force is a constant zero when the generator is disconnected. In other words, no control can be applied during this disconnection period. This restriction makes it impossible to use global optimal control necessary conditions such as the methods of [8] and [11]. Alternatively, the AMMR's optimal control can be formulated as a mixed integer optimal control problem and solved using the relaxing method suggested in [9]. However, the resulting complementarity constraint makes the optimization problem hard to solve. The convergence of gradient-based optimizers is not guaranteed for such problems. And it can easily converge to infeasible points. Therefore, this method is difficult to be implemented in real-time control.

In this paper, a new numerical method based on dynamic programming (DP) is proposed to approximately solve the optimal control of a vibration energy harvester with an AMMR PTO. Dynamic programming has been used in model predictive control of wave energy converters and showed tractable computation complexity [12]. For the AMMR problem, DP's discretization of state spaces and time horizon provides a tractable way to simulate different switching decisions within a bounded time. A novel multi-step DP algorithm is proposed to simultaneously optimize switching times and control forces. The algorithm's computational time is bounded by the discretization resolution. Therefore, the

L. Yang, X. Li and L. Zuo are with the Department of Naval Architecture and Marine Engineering, University of Michigan, Ann Arbor, MI 48109 USA (e-mail: leizuo@umich.edu).

algorithm is guaranteed to return a solution within specified time and thus suitable for real-time control implementation.

The paper is organized as follows. Section 2 describes the AMMR model and formulates the optimal control problem. Section 3 presents the new DP method to solve the problem. Section 4 shows a numerical example to demonstrate the proposed method's effectiveness and Section 5 concludes the paper.

II. PROBLEM FORMULATION

A. AMMR PTO Modelling with an Energy Harvester

The AMMR PTO, in its simplest form, comprises two controllable clutches and a generator. A vibration energy harvester can have translational or rotational oscillatory motions, but both can be transformed to the rotational motion of the generator shaft through some gear transmissions. Therefore, a generic and simplified model of the AMMR energy harvester is presented in Fig. 1 for the formulation of the control problem.

The main component of a vibration energy harvester is an oscillator subject to external excitations. This oscillator's states generally include its position and velocity, and its dynamics can be represented as:

$$\dot{\mathbf{x}} = \mathbf{f}(\mathbf{x}, w) \tag{1}$$

where \mathbf{x} is the state of the oscillator including its position θ and velocity ω , and w is the external force acting on the oscillator. Physically there are three operation statuses of the AMMR PTO as shown in Fig. 1. When positively engaged, the generator's velocity equals the oscillator's velocity, while the polarity is reversed when negatively engaged. Essentially, during these two statuses the generator and the oscillator move together as a rigid body, and the harvested power equals $-\omega u$, where u is the electromagnetic force controlled by the generator. Note that since both u and ω reverse polarity during negative engaging, the power expression remains unchanged. Therefore, the same dynamics equation can be used for both engaging statuses when optimizing the power:

$$\dot{\mathbf{x}} = \mathbf{f}_{en}(\mathbf{x}, f_e, u) \tag{2}$$

where f_e is the external excitation force acting on the oscillator and is the main source injecting energy into the system. At disengaging status, the oscillator and the generator become two separate systems. The oscillator's motion is only driven by the external excitation as:

$$\dot{\mathbf{x}} = \mathbf{f}_{de}(\mathbf{x}, f_e) \tag{3}$$

The generator continues to rotate and generate power that equals $-\omega_{gen}u$. The generator's dynamics in its simplest form is just a first order inertia under control, but it can also consider more realistic scenarios accounting for mechanical losses such as gears' damping and bearings' friction. Since the generator's rotation is mostly unidirectional, only its velocity is of concern in its dynamics:

$$\dot{\omega}_{gen} = f_{gen}(\omega_{gen}, u) \tag{4}$$

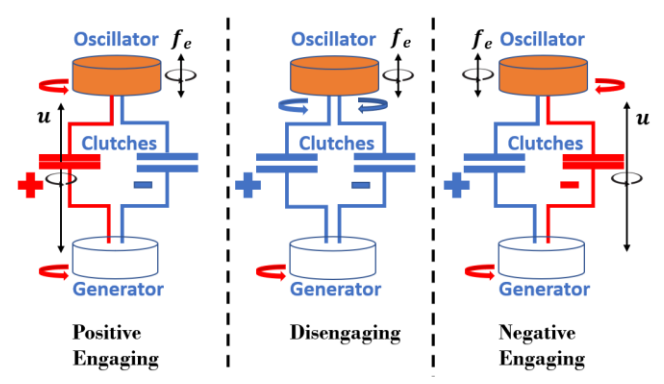


Figure 1. AMMR PTO modelling with a vibration energy harvester

B. Energy Maximization Problem with Prediction

Assuming $f_e(t)$ is known for the time horizon [0,T], the optimal control problem is formulated in (6)-(10). Here, **s** is the switching time vector of the clutches. The admissible set of **s** is defined as:

$$S \triangleq \begin{cases} \mathbf{s} = [s_0, s_1, \dots, s_{n+1}] \in \mathbb{R}^{n+2} \\ s_0 = 0, s_{i-1} \le s_i, s_{n+1} = T, i = 1, \dots, n+1 \end{cases}$$
 (5)

$$\underbrace{\max_{\mathbf{s}\in S, u(t)\in [u_{lb}, u_{ub}]}} = \sum_{i=0}^{n} \int_{s_i}^{s_{i+1}} -\omega_{gen}(t)u(t)dt$$
 (6)

s.t.
$$\dot{\mathbf{x}} = \mathbf{f}_{en}(\mathbf{x}, f_e, u), t \in [s_i, s_{i+1}), i = 0, 2, 4...$$
 (7)

$$\dot{\mathbf{x}} = \mathbf{f}_{de}(\mathbf{x}, f_e), \quad t \in [s_i, s_{i+1}), \quad i = 1, 3, 5...$$
 (8)

$$\dot{\omega}_{gen} = f_{gen}(\omega_{gen}, u), \quad t \in [s_i, s_{i+1}), \quad i = 1, 3, 5...$$
 (9)

$$\omega_{gen} \ge \omega_0$$
 (10)

Note that for this problem the rectification constraint is explicitly enforced in (10) and ω_{θ} is the minimum speed threshold for the generator. Equation (7)-(9) assumes that the AMMR is in engaging status at time 0. If in disengaging status at time 0, the indexes of s need to be swapped between (7) and (8)(9).

Remark 1: When the AMMR's status transitions from disengaging to engaging, an impact will occur to synchronize the speeds at the two sides of the clutch. This impact will cause state jump which needs to be described by separate dynamics. To reduce complications, it's assumed the generator is always controlled to be at the same speed as the oscillator before clutch engaging. Avoiding impacts is also beneficial to the device's reliability.

Remark 2: To fulfill the rectification requirement, the generator needs to be at least disengaged every time before the oscillator's velocity crosses zero. The number of velocity zero crossings in the optimization horizon depends on the excitation force and the applied control, and thus is not known in advance. Switching number n in (5) is chosen as an upper bound of possible switches in the optimization horizon. It's anticipated that if fewer switches are better, some components of the optimal switching time vector \mathbf{s} will turn out to have the same values.

III. METHODOLOGY

A. Problem Discretization

Due to the need to simultaneously optimize switching time s and generator control u, the optimal control problem (6)-(10) is hard to solve analytically and some numerical methods have to be taken. Therefore, first a discretization of the original problem is presented in (11)-(16). The time horizon [0,T] is discretized by a time resolution of Δt , with N Δt =T. The excitation and control are discretized in a zero-order hold way with k denoting the time index such that $t_k=k\Delta t$. The discretization resolution should be at least an order of magnitude higher than the highest dominant frequency of the excitation signal to be representative of the original problem.

$$\max_{\mathbf{s_d} \in S_d, u(k) \in [u_{lb}, u_{ub}]} = \sum_{\mathbf{s_d} \in S_d, u(k) \in [u_{lb}, u_{ub}]} \sum_{i=0}^{n} \sum_{k=s_d^{i-1}}^{s_d^{i+1}-1} -[\omega_{gen}(k) + \omega_{gen}(k+1)]u(k)\Delta t / 2 \qquad (11)$$
s.t.
$$\mathbf{x}(k+1) = \mathbf{f_{en}^d}(\mathbf{x}(k), f_e(k), u(k))$$

$$k \in [s_d^i, s_d^{i+1}), \quad i = 0, 2, 4...$$
(12)

$$\mathbf{x}(k+1) = \mathbf{f}_{de}^{d}(\mathbf{x}(k), f_{e}(k))$$

$$k \in [s_{d}^{i}, s_{d}^{i+1}), \quad i = 1, 3, 5...$$
(13)

(12)

$$\omega_{gen}(k+1) = f_{gen}^d(\omega_{gen}(k), u(k))$$

$$k \in [s_d^i, s_d^{i+1}), i = 1, 3, 5...$$
 (14)

$$\omega_{gen}(k) \ge \omega_0$$
 (15)

$$S_{d} \triangleq \begin{cases} \mathbf{s_{d}} = [s_{d}^{0}, s_{d}^{1}, \dots, s_{d}^{n+1}] \in \mathbb{Z}^{n+2} \\ s_{d}^{0} = 0, s_{d}^{i-1} \le s_{d}^{i}, s_{d}^{n+1} = \mathbb{N}, i = 1, \dots, n+1 \end{cases}$$
(16)

B. Multi-step Dynamic Programming Algorithm

Dynamic programming is a powerful tool for solving sequential optimization problems which include discrete optimal control problems. The essence of the method is to discretize the state space of the system at each time step and optimize the cost of each discretized state at each step in a stepby-step recursive way. The recursive process can start from the initial time moving forward or from the end time moving backward. For the energy maximization optimal control problem, since there are no terminal constraints for states at the end time, and the state at the initial time is given, a forward dynamic programming process is more suitable.

First, a special case of the problem is considered to illustrate the conventional DP process. When n=0 and $s_d =$ [0,N], there is no clutch switching for the entire optimization horizon. In such a case only the generator control u needs to be optimized for each time step. The DP recursive relation is then governed by the Bellman equation (17), where $J_a(\mathbf{x})$ is the maximal energy that can be obtained when the oscillator moves from the initial state \mathbf{x}_0 at time step 0 to the state \mathbf{x} at step q. Note that since the generator is always engaged for this case, $\omega_{gen} = \omega$. **z** belongs to the set of states at step k-1 that can reach the state x via an admissible control. L_s is the single step energy obtained when applying that control. ω_z and ω_x are the velocity components of states z and x. Knowing the optimal energy as a function of states at the current step, the optimal energy at the next step can be solved as a single step optimal control problem. In practice, when analytical derivation of the optimal control is hard to solve from (17), an efficient recursive numerical method can be applied using states and control discretization.

$$J_{q}(\mathbf{x}) = \max_{u(q-1)\in[u_{lb},u_{ub}]} (L_{s}(\mathbf{z},u(q-1)) + J_{q-1}(\mathbf{z}))$$
s.t.
$$\mathbf{x} = \mathbf{f}_{en}^{d}(\mathbf{z}, f_{e}(q-1), u(q-1))$$

$$L_{s}(\mathbf{z}, u(q-1)) = -[\omega_{\mathbf{z}} + \omega_{\mathbf{x}}]u(q-1)\Delta t / 2$$
 (17)

Let the state space be discretized as a grid set $X_d = \{x_d^1,$ $\mathbf{x}_d^2, \dots, \mathbf{x}_d^M$, and the control be discretized as the set $\mathbf{U}_d = \{u_d^1, u_d^2, \dots, u_d^P\}$ with $u_d^1 = u_{lb}$ and $u_d^P = u_{ub}$. The recursive algorithm is summarized in Algorithm 1.

Algorithm 1: Forward Optimization (Single step)

```
For k = 0 to N-1
2
                  For every index m in R(k)
3
                         Eaccu = Emap(m,k);
4
                                For every u<sub>d</sub> in U<sub>d</sub>
5
                                       \mathbf{x}_e = \mathbf{f}_{en}^{\phantom{en}d}(\mathbf{x}_d^{\phantom{dm}}, \mathbf{f}_e(\mathbf{k}), \mathbf{u}_d); \text{ Add } [\mathbf{x}_e] \text{ to } \mathbf{R}(\mathbf{k}+1);
6
                                       Energy = L_s(\mathbf{x_d}^m, \mathbf{u_d})+Eaccu;
7
                                       If Energy > Emap([x_e],k+1)
8
                                              Emap([x_e],k+1) = Energy;
9
                                              Tracemap([\mathbf{x}_e], \mathbf{k+1}) = m; \mathbf{Umap}([\mathbf{x}_e], \mathbf{k+1}) = \mathbf{u}_d;
                                       Endif
10
11
12
                  Endfor
13
```

The process moves from step 0 to step N-1 and the intermediary optimization results are stored in four maps for resolving the optimal control later on. The reachability map R stores the indexes of the reachable states at each step. The optimal energy map Emap stores the optimal energy associated with each state at each step. The trace map Tracemap stores the index of the state at the last step leading to the optimal energy of a state at the current step. The control map Umap stores the optimal control leading to a state at the current step. At each time step, each feasible control is applied to each reachable state through the dynamics on line 5 in Algorithm 1. The resulting state xe at the next step is quantized to a discrete state and its index [xe] is stored as a reachable state. Meanwhile, the accumulated energy of applying this control is compared to the maximal energy stored in the energy map. If it exceeds the existing maximum, the energy, trace, and control maps are updated to record the new optimum. After the forward process finishes and all the storage maps are propagated, the optimal trajectories can be easily resolved from a backward tracing process shown in Algorithm 2.

Algorithm 2: Backward Tracing (Single step)

```
1
     Find idx = argmax_m Emap(m,N); k = N;
     While k > 0
2
             \mathbf{xopm}(\mathbf{k}) = \mathbf{x_d}^{idx};
3
4
             \mathbf{uopm}(k-1) = \mathbf{Umap}(idx,k);
5
             idx = Tracemap(idx,k);
6
             k = k-1;
     End
```

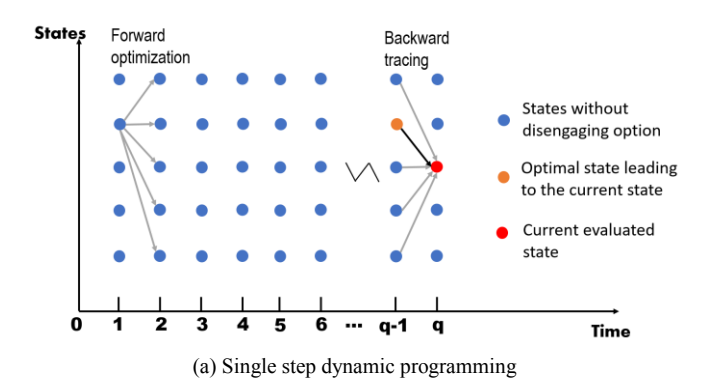
The primary distinction of the general problem (11)-(16) from the always engaging case is the added option of another control action at each step, i.e. disengaging the generator. If continuing to use the single step DP in (17), three troublesome issues will arise. First, a separate state is required to describe the generator speed as it will not equal the oscillator velocity. Second, the number of controls at each step will double due to the binary option of engaging/disengaging. These two issues will significantly increase computation time especially if the discretization resolution is high. Another issue is that there will be no restrictions on the length of interval between switching. The switching frequency can get as high as $1/\Delta t$ and may add unnecessary burden to the clutches for marginal energy increase. For these reasons, a modified multi-step DP relation is proposed in (18).

$$\begin{split} & \mathbf{Max}_{k \in T(\mathbf{x},q)} \begin{bmatrix} \max_{u(k) \in [u_{lb},u_{ub}]} (L_s(\mathbf{z},u(k)) + J_k(\mathbf{z})), k = q - 1 \\ \max_{\mathbf{z} \in R_k} (L_m(\mathbf{z},\mathbf{x}) + J_k(\mathbf{z})), k < q - 1 \end{bmatrix} \\ & \text{s.t.} \quad \mathbf{x} = \mathbf{f_{en}^d}(\mathbf{z}, f_e(k), u(k)), \qquad k = q - 1 \\ & \mathbf{x}_k = \mathbf{f_{de}^d}(\mathbf{z}, f_e(k-1)), \text{ and } \qquad k < q - 1 \\ & \mathbf{x}_{k+1} = \mathbf{f_{de}^d}(\mathbf{x}_k, f_e(k)), \dots, \mathbf{x} = \mathbf{f_{de}^d}(\mathbf{x}_k, f_e(q-1)) \end{split}$$

For this modified equation, one state can be reached from either the last step or multiple steps back. When it is reached from the last step, the current status remains engaging and the optimal energy is computed in the same way as the single step DP. When it is reached from an earlier step, the current status changes from disengaging to engaging. The optimal energy during the multistep disengaging span is represented as Lm. The optimal trajectory for an oscillator state is chosen from all the previous steps T(x,q) that can reach that state. The key insight that leads to this method is that Lm can be expressed analytically. During disengagement, the generator is a first order inertia converting its kinetic energy to electricity. When assuming reengaging at the same speed with the oscillator, the maximal energy recovered during disengagement is simply the kinetic energy drop of the generator inertia. When the generator's losses are considered, Lm can still be explicitly expressed either by solving an optimal control for a generator model or adding an efficiency coefficient.

Fig. 2 illustrates how the multistep DP works and compares it with the single step DP. For multistep DP, not all the states have the option of disengaging at any time, instead a set of disengaging rules dictates which states can disengage. This allows restrictions to be placed on the switching pattern and reduces computation loads. When executing the disengaging action, a forward simulation is performed until reengaging conditions are met. The reengaging conditions are set such that rectification constraints are satisfied. Energy is directly computed for the disengaging steps without the need of step by step control optimization, keeping the computation tractable.

Essentially, the multistep DP process allows some switching rules to be enforced within the DP framework. These rules reduce exploration spaces and promote more practical switching patterns. More strict rules lead to less



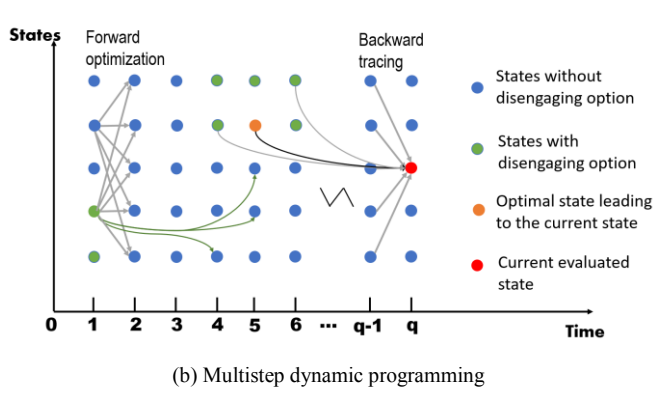


Figure 2. Illustrations of single step and multistep dynamic programming

computation time and more predictable switching patterns, while looser rules more closely approximate the true energy optimum at the cost of more computation time and less favorable switching patterns. In this work, a set of rules based on the oscillator's velocity is proposed as an example. The corresponding multistep DP algorithm is presented in Algorithm 3. In the pseudocode $g(\mathbf{x})$ is a function outputting the oscillator's velocity from its state. Compared with Algorithm 1, the main difference of Algorithm 3 is the added branch of disengaging action from line 17-40. The disengaging rules are set based on several discrete speed thresholds (only two are showed in the pseudocode). Basically, the generator can be disengaged when its speed drops below a threshold if its peak speed exceeds the threshold before. This is to ensure that disengaging happens when the oscillator's speed decreases and is about to reverse direction. An additional Peakmap storage is needed to record the peak speed during the engaging status. From line 19-39, the oscillator's states are continuously simulated until either its speed exceeds the maximal reengaging speed Vre2 or the prediction horizon ends. During this simulation, reengaging is allowed after the oscillator's velocity crosses zero and exceeds the minimal reengaging speed Vre1. The state after reengaging is marked as a reachable state and the associated storage maps are updated. Note a new Tmap is introduced to record the time step leading to the reengaging state, which will be used in the multistep backward tracing. The rules chosen in this algorithm restrict the switching to happen just for rectification (disengaging at velocity zero crossing). By setting Vre1 $\geq \omega_0$ and Vth2>Vth1> ω_0 , the minimal generator speed constraint (15) is also satisfied. After the forward optimization finishes, the optimal control sd and uopm can be resolved in a backward tracing process shown in Algorithm 4.

IV. RESULTS

The proposed control method is tested on a simplified wave energy converter model with the AMMR PTO. The WEC's wave capture structure typically has the same dynamics as a spring-mass-damper (SMD) system under harmonic wave excitations. With panchromatic irregular waves, the oscillating capture structure's dynamics is more complex, generally needing to be approximated by a higher order model. For this study, a second order SMD model is used to represent the WEC oscillator's dynamics. Second order model can match the WEC dynamics within a frequency range. Since the wave excitation spectrum typically has a narrow band, a second order model can be tuned to match the WEC dynamics at the frequency range where the wave power is concentrated. The parameters chosen for the model in this paper roughly match an oscillating surge device around its resonant frequency [13]. The buoyancy spring coefficient is 300 Nm/rad. The physical mass and added mass combined are 70 Kgm². The radiation damping is 60 Nms/rad. The device parameter is then scaled up 5 times using the Froude law. The model assumes perfect clutches engaging/disengaging happens instantaneously. mechanical friction and damping are lumped to 140 Nms/rad, adding to the radiation damping. The generator's inertia is 50 Kgm² after equivalized with the gear ratio. The generator torque range after multiplied by the gear ratio is from -2000 Nm to 2000 Nm. The control torque is discretized to 400 levels. The two states for second order systems are just position and velocity. The position of a surge device is restricted to ± 30 degrees and discretized equally to 701 states. The velocity is restricted to ± 1 rad/s (± 66 rad/s after gear ratio) and discretized to 801 states. The excitation wave is generated from a JONSWAP spectrum with a peak period of 6.7s and a significant wave height of 1 m. The prediction horizon for the wave excitation torque is set as 15s with a discretization of 0.1s time steps. A 300s realization of excitation torque is used to test the control algorithm shown in Fig. 3. Both single step DP and multistep DP are tested for the excitation profile.

A typical portion of the resulting optimal trajectories are shown in Fig. 4 and Fig. 5. The excitation and control are normalized to be plotted together with the WEC wave capture structure's velocity. Note the WEC velocity is after a 1:66 gear ratio. For the case of AMMR, the generator is disengaged when the control is zero. It is observed in Fig. 5 that most of the time the generator is disengaged when the WEC's velocity crosses zero, meaning the rectification requirement is satisfied. Note in this case study sometimes the generator is not disengaged and reverses direction. This is because the rules are set such that rectification is only compulsory when the generator's peak speed has exceeded a threshold. Experiments show that generator efficiency is low below certain speeds and little can be gained from rectification.

Compare Fig. 4 and Fig. 5, the similarity is that both controls align the WEC's velocity with the excitation torque. This phase alignment maximizes the energy input from the wave to the WEC. By examining the control actions in detail, it is found that the non-switching case involves more reactive power flow, which often happens after velocity zero crossings. (Reactive power is the power injected into a WEC by the generator when the control and velocity have the same sign.)

Algorithm 3: Forward Optimization (Multistep)

```
For k = 0 to N-1
2
              For every index m in R(k)
3
                    Eaccu = Emap(m,k); Vp = Peakmap(m,k); Vs = |g(x_d^m)|;
4
                         For every u<sub>d</sub> in U<sub>d</sub>
5
                              \mathbf{x}_e = \mathbf{f}_{en}^{\ d}(\mathbf{x}_d^{\ m}, \mathbf{f}_e(\mathbf{k}), \mathbf{u}_d); \text{ Add } [\mathbf{x}_e] \text{ to } \mathbf{R}(\mathbf{k}+1);
6
                              Energy = L_s(\mathbf{x_d}^m, \mathbf{u_d})+Eaccu;
                              If Energy > Emap([x_e],k+1)
8
                                    Emap([x_e],k+1) = Energy;
                                    Tracemap([\mathbf{x}_e], \mathbf{k}+1) = m; Umap([\mathbf{x}_e], \mathbf{k}+1) = u<sub>d</sub>;
9
                                    newp = max(|g(\mathbf{x}_e)|, Vp);
10
                                   If newp > Peakmap([x_e],k+1)
11
12
                                     Peakmap([\mathbf{x}_e], k+1) = newp;
13
                                   Endif
14
                                   Tmap([x_e],k+1) = k;
15
                              Endif
16
                        Endfor
17
                    If (Vp > Vth1 \& Vs \le Vth1) || (Vp > Vth2 \& Vs \le Vth2)
18
                         V_S = 0; zcro = 0; kk = k; x_s = x_d^m;
19
                         While (V_s < V_{re2} \parallel z_{cro} == 0) & k_k < N
20
                              \mathbf{x}_e = \mathbf{f}_{de}^{d}(\mathbf{x}_s, \mathbf{f}_e(kk)); \quad V_S = |\mathbf{g}(\mathbf{x}_e)|;
                              If zcro = 0
21
22
                                    If sign(g(\mathbf{x}_e)) \sim = sign(g(\mathbf{x}_s))
23
                                      zcro == 1;
24
                                   Endif
25
                              Elseif zcro == 1
26
                                   If Vs \ge Vre1
27
                                         Add [\mathbf{x}_e] to \mathbf{R}(kk+1);
28
                                         Energy = L_m(\mathbf{x_d}^m, \mathbf{x_e})+Eaccu;
29
                                         If Energy > Emap([x_e],kk+1)
30
                                              Emap([x_e],kk+1) = Energy;
31
                                              Tracemap([\mathbf{x}_e],kk+1) = m;
32
                                              Umap([x_e],kk+1) = 0;
33
                                              Peakmap([x_e],kk+1) = |g(x_e)|;
34
                                              Tmap([x_e],kk+1) = k;
35
                                         End
36
                                   Endif
37
                              Endif
38
                             \mathbf{x}_{s} = \mathbf{x}_{e}; kk = kk+1;
39
                        Endwhile
40
                    Endif
41
              Endfor
42
         Endfor
```

Algorithm 4: Backward Tracing (Multistep)

```
Find idx = argmax_m Emap(m,N);
        k = N; s_d = 0; k_S = n+2; s_d(k_S) = N;
2
3
        While k > 0
4
            kc = k; xopm(kc) = x_d^{idx};
            \mathbf{uopm}(kc-1) = \mathbf{Umap}(idx,kc);
5
            idx = Tracemap(idx,kc);
6
7
            k = Tmap(idx,kc);
8
            If k \le kc-1
9
                k_S = k_{S-1}; s_d(k_S) = k_C;
                k_S = k_{S-1}; s_d(k_S) = k;
10
            Endif
11
12
        End
```

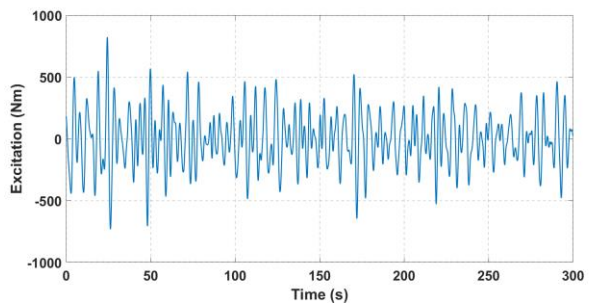


Figure 3. A JONSWAP irregular wave excitation sequence

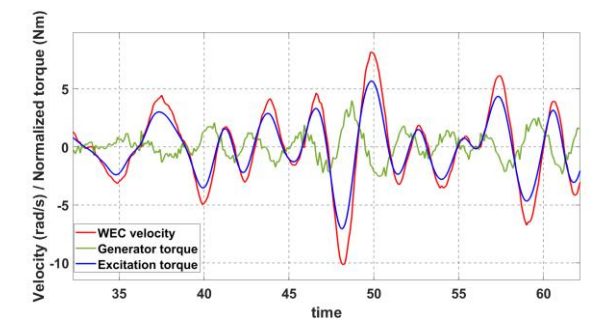


Figure 4. Non-switching optimal trajectories (single step DP)

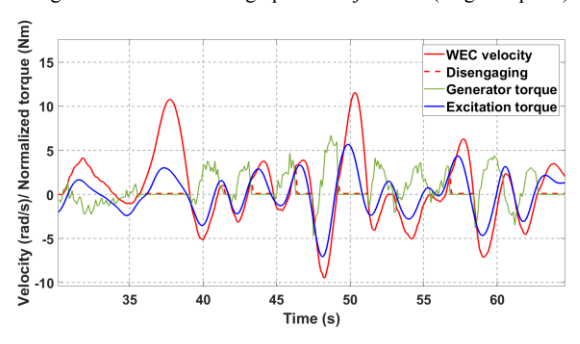


Figure 5. AMMR optimal trajectories (multistep DP)

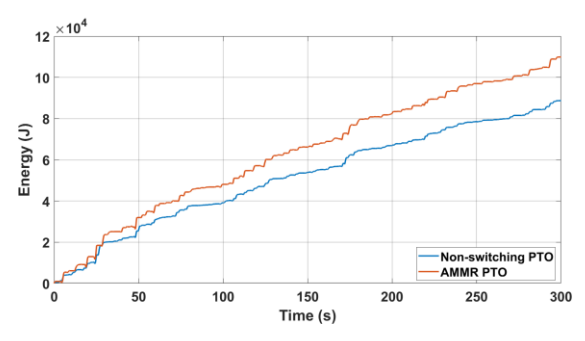


Figure 6. Energy comparison between conventional and AMMR PTO

On the other hand, in the AMMR case there is no such reactive power around zero crossings. While reactive power is still observed for smaller waves, the generator mostly operates in the active power mode (control and velocity have an opposite sign) for larger waves. Fig. 6 shows the accumulated energy of a conventional linear PTO versus an AMMR PTO. It can be seen the AMMR PTO increases power by around 30% through the proposed multistep DP algorithm.

V. CONCLUSION

In this paper, a challenging optimal control problem arising

from a promising new vibration energy harvesting PTO is formulated rigorously and tackled numerically. The problem involves switching systems and requires simultaneous optimization of switching times and control. A numerical solution framework based on dynamic programming is proposed to solve the problem approximately. The framework is designed to be flexible to accommodate different switching rules to satisfy complex rectification constraints. An example control algorithm using the framework is detailed and implemented to a simplified WEC system. Preliminary results show the algorithm effectively maximizes energy while successfully performing rectification for the AMMR PTO. More work will be done in the future to consider more realistic generator models, evaluate discretization errors and demonstrate the control algorithm in hardware.

ACKNOWLEDGMENT

The authors wish to thank the financial support from US NSF Grant # 2152694.

REFERENCES

- [1] Henderson, R. (2006). Design, simulation, and testing of a novel hydraulic power take-off system for the Pelamis wave energy converter. *Renewable energy*, 31(2), 271-283.
- [2] Dang, T. D., Phan, C. B., & Ahn, K. K. (2019). Modeling and experimental investigation on performance of a wave energy converter with mechanical power take-off. *International Journal of Precision Engineering and Manufacturing-Green Technology*, 6, 751-768.
- [3] Li, X., Chen, C. A., Chen, S., Xiong, Q., Huang, J., Lambert, S., ... & Zuo, L. (2022). Dynamic characterization and performance evaluation of a 10-kW power take-off with mechanical motion rectifier for wave energy conversion. *Ocean Engineering*, 250, 110983.
- [4] Cargo, C. J., Hillis, A. J., & Plummer, A. R. (2016). Strategies for active tuning of Wave Energy Converter hydraulic power take-off mechanisms. *Renewable Energy*, 94, 32-47.
- [5] Li, Z., Zuo, L., Kuang, J., & Luhrs, G. (2012). Energy-harvesting shock absorber with a mechanical motion rectifier. *Smart materials* and structures, 22(2), 025008.
- [6] de Oliveira, L., dos Santos, I. F. S., Schmidt, N. L., Tiago Filho, G. L., Camacho, R. G. R., & Barros, R. M. (2021). Economic feasibility study of ocean wave electricity generation in Brazil. *Renewable Energy*, 178, 1279-1290.
- [7] Yang, L., Huang, J., Congpuong, N., Chen, S., Mi, J., Bacelli, G., & Zuo, L. (2021). Control Co-design and Characterization of a Power Takeoff for Wave Energy Conversion based on Active Mechanical Motion Rectification. *IFAC-PapersOnLine*, 54(20), 198-203.
- [8] Xu, X., & Antsaklis, P. J. (2004). Optimal control of switched systems based on parameterization of the switching instants. *IEEE* transactions on automatic control, 49(1), 2-16.
- [9] Bengea, S. C., & DeCarlo, R. A. (2005). Optimal control of switching systems. *automatica*, 41(1), 11-27.
- [10] Shaikh, M. S., & Caines, P. E. (2007). On the hybrid optimal control problem: theory and algorithms. *IEEE Transactions on Automatic Control*, 52(9), 1587-1603.
- [11] Fu, J., & Zhang, C. (2021). Optimal control of path-constrained switched systems with guaranteed feasibility. *IEEE Transactions on Automatic Control*, 67(3), 1342-1355.
- [12] Li, G., Weiss, G., Mueller, M., Townley, S., & Belmont, M. R. (2012). Wave energy converter control by wave prediction and dynamic programming. *Renewable energy*, 48, 392-403.
- [13] Ahmed, A., Yang, L., Huang, J., Shalaby, A., Datla, R., Zuo, L., & Hajj, M. (2024). Performance characterization and modeling of an oscillating surge wave energy converter. Nonlinear Dynamics, 112(6), 4007-4025.